Polymer Chemistry

PAPER

View Article Online
View Journal | View Issue

Cite this: *Polym. Chem.*, 2016, **7**, 2395

Hydrogen bonding strength effect on self-assembly supramolecular structures of diblock copolymer/homopolymer blends†

Shih-Chi Tsai, Yung-Chih Lin, En-Li Lin, Yeo-Wan Chiang and Shiao-Wei Kuo*

Received 2nd February 2016,
Accepted 2nd March 2016

DOI: 10.1039/c6py00195e

www.rsc.org/polymers

In this study we investigated the steric hindrance effect on the hydrogen bonding strength and self-assembly supramolecular structures of the poly(styrene-*b*-vinylphenol) (PS-*b*-PVPh) diblock copolymer when blended with the homopolymers poly(4-vinylpyridine) (P4VP) and poly(2-vinylpyridine) (P2VP). Each of these PS-*b*-PVPh/P4VP and PS-*b*-PVPh/P2VP blends underwent a sequence of order–order morphological transitions with wet-brush behavior from lamellae to hexagonally packed cylindrical to spherical structures. Interestingly, we observed a bicontinuous gyroid structure only in the more strongly hydrogen bonding PS-*b*-PVPh/P4VP blend. Furthermore, the PS-*b*-PVPh/P4VP blend exhibited its order–order morphological transitions at relatively low homopolymer concentrations and did not display a two-phase region at relatively high homopolymer concentrations. Thus, differences in the steric bulk of the homopolymers P4VP and P2VP affected their hydrogen bonding with the diblock copolymer PS-*b*-PVPh and, therefore, influenced the self-assembled structures formed from their blends.

Introduction

The self-assembly of supramolecular structures from diblock copolymers has received much attention because such materials have potential applications in, for example, drug delivery, photovoltaic devices, and photonic crystals.[1–5] Various self-assembled morphologies can be formed from diblock copolymers in the bulk state, including lamellae, bicontinuous gyroids, hexagonally packed cylinders, and spherical structures; in solution they can form spherical, worm-like, and vesicle micelle structures.[6–8] The types of self-assembled structures that can form in the bulk state are strongly dependent on the Flory–Huggins interaction parameters, the molecular weights (degrees of polymerization), and the volume fractions of the block segments.[9–11] Although different self-assembled nanostructures in the bulk state can be synthesized by varying the volume fraction or the molecular weights of each block segment, this approach can be time-consuming and expensive. Therefore, the blending of a diblock copolymer (A-*b*-B) with a homopolymer (A, B, or C), as a way of varying the volume fraction of each block segment, has drawn much attention recently as a way of preparing unusual self-assembled nanostructures.[12–17]

In the first case, proposed by Hashimoto *et al.*, the blending of a diblock copolymer (A-*b*-B) with the A or B homopolymer can lead to structures undergoing order–order morphological transitions or macrophase separation, processes strongly affected by the molecular weight of the A or B homopolymer.[12,13] Three categories have been proposed based on the molecular weight ratios of the A homopolymer and the A block segment ($a = M_{h\text{-}A}/M_{b\text{-}A}$): (i) complete macrophase separation ($a \gg 1$), (ii) a "dry brush" system ($a \sim 1$), and (iii) a "wet-brush" system ($a < 1$).[12,13] Blending of an A homopolymer would lead to homogeneous dissolving in the A block copolymer segment, resulting in a domain size change or even an order–order morphological transition in the wet-brush system.

In the second case, the blending of the diblock copolymer (A-*b*-B) with the C homopolymer can lead to other interesting self-assembled nanostructures.[18–51] Four different possibilities exist, and have been examined either experimentally or theoretically, that C is miscible with the A or B block in A-*b*-B/C blends.[18–48] The simplest and most investigated possibility is that the A and B block segments are immiscible, whereas C is miscible (*via* hydrogen bonding) with the B block but is immiscible with the A block.[18–25] Kwei *et al.* proposed the initial concept of blending the diblock copolymer PS-*b*-PVPh with various hydrogen bond-accepting homopolymers such as poly(4-vinyl pyridine) (P4VP), poly(ethylene oxide) (PEO), and poly(methyl methacrylate) (PMMA).[18] The OH groups of the

Department of Materials and Optoelectronic Science, Center for Functional Polymers and Supramolecular Materials, National Sun Yat-Sen University, Kaohsiung, Taiwan. E-mail: kuosw@facuty.nsysu.edu.tw

†Electronic supplementary information (ESI) available. See DOI: 10.1039/c6py00195e

PVPh block can hydrogen bond intermolecularly with these hydrogen bond-accepting homopolymers, but these homopolymers should be immiscible with the PS block segment; although microphase separation was expected, it was not reported in that study.[18] Ikkala *et al.* reported the first self-assembled lamellae structures formed upon blending the diblock copolymer poly(isoprene)-*b*-poly(2-vinyl pyridine) (PI-*b*-P2VP) with a phenolic homopolymer; the phenolic was miscible with the P2VP block through the hydrogen bonding interactions, but it was immiscible with the PI block.[19] Matsushita *et al.* systematically studied the blending of the diblock copolymer PS-*b*-P2VP with the PVPh homopolymer of various molecular weights; whereas PVPh is miscible with the P2VP block through the hydrogen bonding interaction, it is immiscible with PS, resulting in order–order morphological transitions upon increasing the concentration of PVPh.[20–22]

Previously, we examined the blending of the diblock copolymer PS-*b*-PVPh with two well-known hydrogen bonded acceptor homopolymers, P4VP and PMMA, which form hydrogen bonds of different strengths in the B/C inter-polymer complexes.[24] We observed order–order morphological transitions or wet-brush behavior from lamellae to bicontinuous gyroids to hexagonally packed cylinders and finally to the spherical structure upon increasing the concentration of the P4VP homopolymer, but no morphological transition (dry-brush behavior) and macrophase separation in the PS-*b*-PVPh/PMMA blends at relatively high PMMA concentrations. This behavior was due to the different strengths of hydrogen bonding interactions in PVPh/P4VP and PVPh/PMMA blend systems; the inter-association equilibrium constants of PVPh/P4VP blends (K_A = 1200) and PVPh/PMMA blends (K_A = 37.4), and the self-association equilibrium constant of pure PVPh (K_B = 66.8) have been determined from the Painter–Coleman association model (PCAM).[52] We proposed that the ratio K_A/K_B (where $K_A > 1$ for PVPh/P4VP, but $K_A/K_B < 1$ for PVPh/PMMA) be used as a parameter to determine the types of self-assembled structures in A-*b*-B/C blends. We concluded that blending with C tends to result in wet-brush-like structures when K_A/K_B is greater than unity (*e.g.*, for PVPh/P4VP) and dry-brush-like structures when K_A/K_B is less than unity (*e.g.*, for PVPh/PMMA). Our experimental findings were consistent with the theoretical model proposed by the Shi group.[25] They used an attractive-interaction model (AIM) to investigate the blending of A-*b*-B block copolymers with C homopolymers; they observed order–order transitions from lamellae to the hexagonally packed cylinder and, finally, to spherical structures upon increasing the homopolymer concentration when strong hydrogen bonding was present. In contrast, they observed immiscibility or macro-phase separation upon increasing the homopolymer concentration in the case of a relatively weak hydrogen bonding region, with the system proceeding from the lamellar structure to the macro-phase separation region. Thus, the strength of hydrogen bonding is a very important parameter affecting the self-assembled structures in A-*b*-B/C blends. Although PVPh/P4VP and PVPh/PMMA blends have clearly different hydrogen bonding strengths, their solubility parameters from the physical force are also different, as determined using the group contribution method [δ = 10.85 (cal mL^{-1})$^{1/2}$ for P4VP; δ = 9.1 (cal mL^{-1})$^{1/2}$ for PMMA].[52]

In the present study we examined the self-assembled structures in A-*b*-B/C blends with different strengths of hydrogen bonding but the same solubility parameter for their hydrogen bond acceptor homopolymers. In previous studies, we had examined the effect of steric hindrance when blending P4VP or P2VP with phenolic resin, stabilized through either hydrogen bonding or metal–ligand coordination with $Zn(ClO_4)_2$.[53,54] P4VP and P2VP have the same solubility parameter (based on the group contribution method) because they are merely isomeric structures. Although the solubility parameter is the same, the self-assembled structures in PS-*b*-P4VP or PS-*b*-P2VP in polar solvents are quite different. Inter-association hydrogen bonding and metal–ligand coordination in P4VP blends are stronger (based on IR analyses) than those in P2VP blends because of the greater steric hindrance about the nitrogen atoms in P2VP.[53,54] For example, the value of K_A for PVPh/P4VP is 1200 whereas for PVPh/P2VP blends it is 598. Although P4VP and P2VP segments have been employed widely in the diblock copolymer to form self-assembled structures with homopolymers or nanoparticles (stabilized through hydrogen bonding or metal–ligand coordination),[55–62] the effect of steric hindrance on hydrogen bonding strength has not been reported to the best of our knowledge.

As a result, the objective of this study was to examine the interactions of a PS-*b*-PVPh diblock copolymer, synthesized through anionic living polymerization, with P4VP and P2VP homopolymers of similar molecular weights and thereby determine the influence of the steric hindrance of the homopolymer on the hydrogen bonding strength. Notably, these PS-*b*-PVPh/P4VP and PS-*b*-PVPh/P2VP blends can still be classified as strong hydrogen bonding blend systems, because both values of K_A are significantly larger than the K_B value of PVPh, even though the hydrogen bonding strengths are different. We used differential scanning calorimetry (DSC), Fourier transform infrared (FTIR) spectroscopy, small-angle X-ray scattering (SAXS), and transmission electron microscopy (TEM) to characterize the phase behavior, hydrogen bonding interaction, and self-assembled structure in these two systems.

Experimental section

Materials

Styrene (99%, Aencore), 4-*tert*-butoxystyrene (*t*BuOS, 99%, Aldrich), 4-vinyl pyridine (4VP, 95%, Acros), and 2-vinyl pyridine (2VP, 97%, Acros) were distilled from CaH_2. THF was distilled from Na/benzophenone after heating under reflux for 3 h under N_2. LiCl was dried at 160 °C in a vacuum oven overnight. The *sec*-BuLi (1.3 M in CHEX, Chemetall) was used as received.

The PS-*b*-PVPh diblock copolymer and P4VP and P2VP homopolymers through anionic living polymerization

Dry LiCl was charged with a THF solution and subsequently cooled to −78 °C under an Ar atmosphere in a glass reactor.

The *sec*-BuLi was then added after 5 min until the solution becomes yellow in color. The solution was warmed to room temperature until it became colorless and then cooled again to −78 °C and then *sec*-BuLi was added. After 5 min, a styrene monomer was added, forming a yellow color again. After 50 min, *t*BuOS was then added through the cannula to the glass reactor. The light yellow color disappeared to provide an orange solution. After 2 h at −78 °C, an excess amount of MeOH was then added to terminate the anionic living polymerization. The block copolymer was precipitated with MeOH and dried under vacuum overnight at 60 °C. The PS-*b*-P*t*BuOS was converted to the PS-*b*-PVPh diblock copolymer through hydrolysis as shown in Scheme 1. PS-*b*-P*t*BuOS dissolved in dioxane and HCl (37 wt%; 10 equiv.) was then added. The solution was stirred overnight under N_2 at 80 °C. The mixture was precipitated from H_2O and then neutralized with NaOH solution (5 wt%) to pH 6–7; the diblock copolymer was filtered off and dried at room temperature in the vacuum oven. The diblock copolymer was subjected to three dissolve/precipitate cycles by using THF and MeOH/H_2O solvent mixtures (v/v = 1 : 1), and then dried in the vacuum oven overnight at 60 °C.

The P4VP and P2VP homopolymers were also synthesized through anionic living polymerizations in the THF solvent at −78 °C by using the *sec*-BuLi as the initiator as shown in Scheme 2. After 5 min, DPE was added to form a deep red color. The 2VP or 4VP monomer was then added through the cannula to the glass reactor. After 2 h at −78 °C, excess amounts of MeOH were then added to terminate the anionic living polymerization. The homopolymers were precipitated with hexane and then dried in the vacuum oven overnight at 60 °C. The molecular weights and polydispersity indices (PDIs) of the PS-*b*-PVPh diblock copolymer, P4VP, and P2VP homopolymers were determined by size exclusion chromatography in DMF (Table 1).

Diblock copolymer/homopolymer blends

PS-*b*-PVPh/P4VP and PS-*b*-PVPh/P2VP blends were prepared through solution blending at various compositions. The 5 wt% DMF solutions of the A-*b*-B/C blends were stirred overnight and the solvents were then slowly evaporated at 90 °C for 3 days; a subsequent drying at 200 °C for 1 week was performed to remove the possible residual DMF.

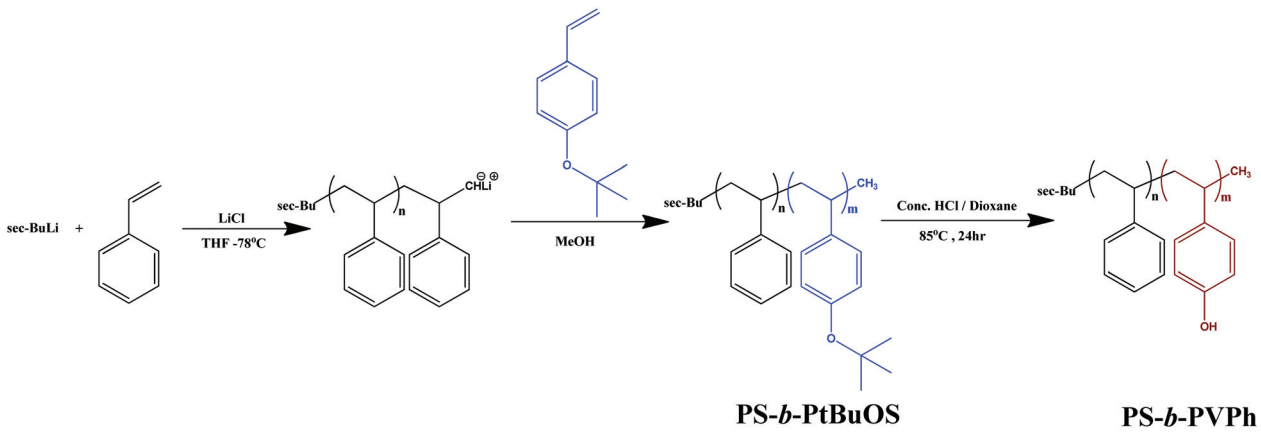

Scheme 1 The synthesis scheme of the PS-*b*-PVPh diblock copolymer used in this study.

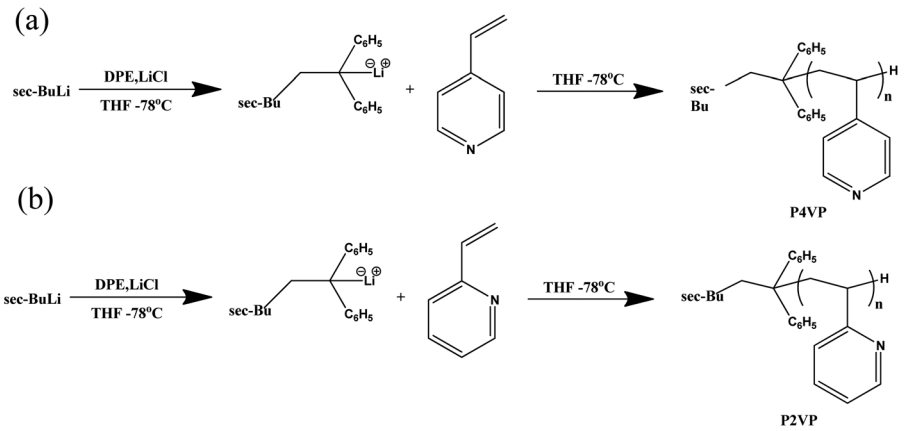

Scheme 2 The synthesis scheme of (a) P4VP and (b) P2VP homopolymers through anionic living polymerization.

Table 1 Characterization data of the homopolymers P4VP and P2VP and the diblock copolymer PS-*b*-PVPh synthesized through anionic living polymerization in this study

Polymer	M_n	M_w/M_n	Volume fraction of PS (%)	Volume fraction of PVPh (%)
PS_{200}-*b*-$PVPh_{93}$ (HS)	31 940	1.08	67.0	33.0
$P4VP_{105}$	11 000	1.04		
$P2VP_{101}$	10 600	1.02		

Characterization

^1H or ^{13}C NMR spectra were recorded at room temperature using a Bruker AM 500 (500 MHz) spectrometer. Molecular weights and PDIs were recorded *via* gel permeation chromatography (GPC) using a Waters 510 high-performance liquid chromatograph with DMF as the eluent (flow rate: 0.6 mL min^{-1}). The narrow polydispersity of polystyrene was the standard. The DSC analyses were performed using a TA-Q20 instrument over the temperature range from −90 to 240 °C at 20 °C min^{-1} heating rate under a N_2 atmosphere. FTIR samples were prepared by the KBr disk method and were suitably thin to obey the Beer–Lambert law; the spectra were recorded using the Bruker Tensor 27 spectrophotometer (32 scans; spectral resolution: 1 cm^{-1}). FTIR spectra were also recorded at various temperatures using a temperature-controlled compartment holder. SAXS analyses were performed by using the BL17A1 wiggler beamline (wavelength: 1.12 Å) at the National Synchrotron Radiation Research Center (NSRRC) in Taiwan. These samples were also analyzed at several temperatures on the hot stage under a N_2 atmosphere. The TEM analyses were performed by using JEOL JEM-2100 apparatus operated at 200 kV accelerating voltage. An ultrathin section of the TEM sample (thickness: *ca.* 70–100 nm) was prepared using a Leica Ultracut UCT Microtome equipped with a diamond knife. The TEM samples were also stained selectively with I_2; thus, the PVPh/P4VP or PVPh/P2VP domains appeared dark, while the PS block segments appeared white.

Results and discussion

Synthesis of the PS-*b*-PVPh diblock copolymer

We reported the synthesis of PS-*b*-PVPh in a previous study;[63,64] we used sequential anionic living polymerization and then a hydrolytic reaction to remove the protecting *tert*-butyl ether group of the poly(*tert*-butoxystyrene) (PtBOS) block segment (Scheme 1). We verified the generation of the OH groups of PS-*b*-PVPh through complete removal of the *tert*-butyl ether protective unit, using ^1H and ^{13}C NMR and FTIR spectroscopy [Fig. 1(A)–(C)]. The signals at 1.30 ppm in the ^1H NMR spectrum [Fig. 1(A)-(a)] and 78.0 ppm in the ^{13}C NMR

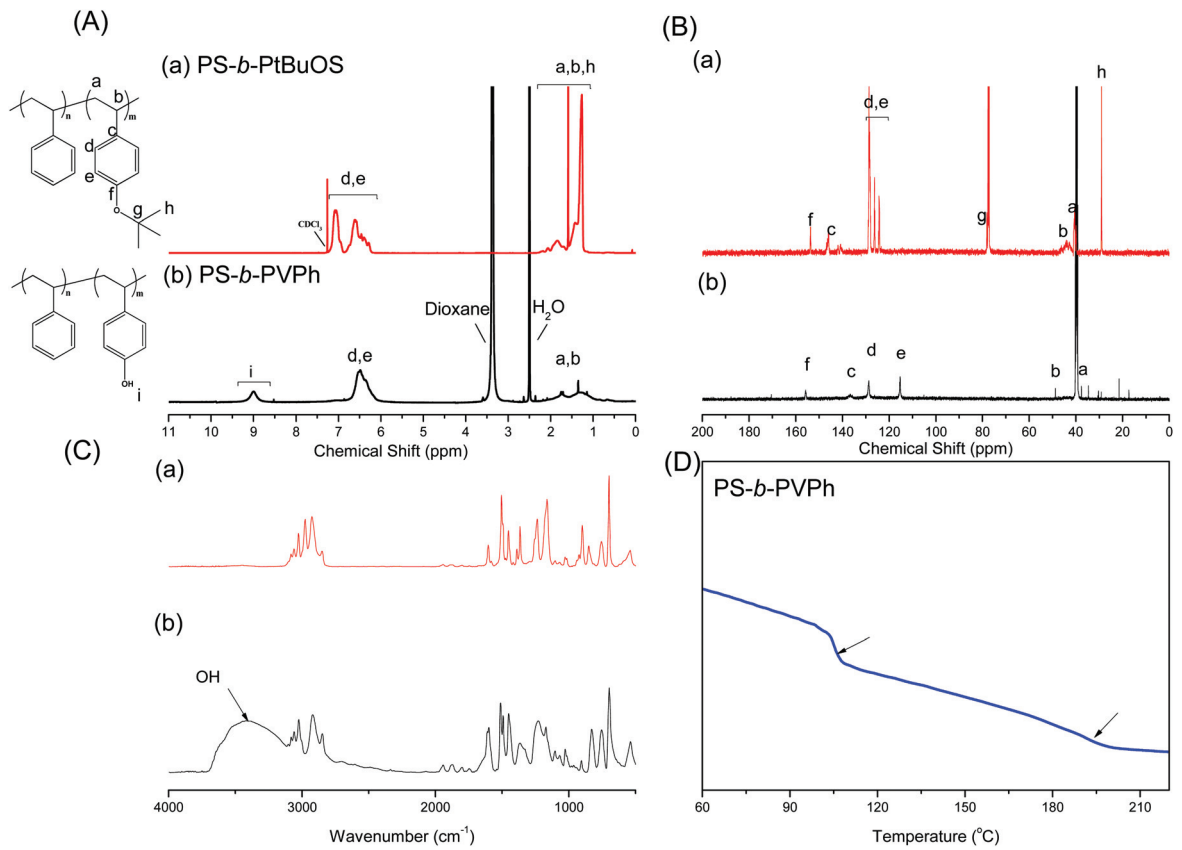

Fig. 1 (A) ^1H NMR, (B) ^{13}C NMR, and (C) FTIR spectra of (a) PS-*b*-PtBuOS and (b) PS-*b*-PVPh. (D) DSC analysis of the PS-*b*-PVPh.

spectrum [Fig. 1(B)-(a)] of the PS-*b*-P*t*BOS diblock copolymer represent the *tert*-butyl ether units. These signals disappeared after hydrolysis, with a signal at 9.0 ppm in Fig. 1(A)-(b) representing the OH groups of the PVPh block segment, while the signal of the (C_f–OH) groups shifted from 153.6 ppm [Fig. 1(B)-(a)] to 155.8 ppm [Fig. 1(B)-(b)], consistent with complete hydrolysis. The same conclusion was drawn from the FTIR spectra. The spectrum of the PS-*b*-PVPh featured a broad signal at 3430 cm^{-1}, representing the OH group formed after deprotection [Fig. 1(C)-(b)]. Fig. 1(D) reveals that the PS-*b*-PVPh diblock copolymer has two glass transition temperatures (T_gs), at 107 °C (PS segment) and 182 °C (PVPh segment), indicative of chemical immiscibility and microphase separation in this diblock copolymer. Based on ^{1}H NMR spectroscopic and GPC analyses, we calculated the volume fraction of PVPh in the PS-*b*-PVPh copolymer to be 35 wt% (33 vol%). Table 1 summarizes the molecular weight and PDI of our PS-*b*-PVPh diblock copolymer and P4VP and P2VP homopolymers. Clearly, the molecular weights of P4VP and P2VP homopolymers are similar with low polydispersity and these two homopolymers are slight larger than PVPh in the block copolymer where $a = M_{h\text{-}A}/M_{b\text{-}A}$ is close to 1.

Thermal analyses of PS-*b*-PVPh/P4VP and PS-*b*-PVPh/P2VP blend systems

Fig. 2 displays the second DSC heating scans of PS-*b*-PVPh/P4VP and PS-*b*-PVPh/P2VP blends. The pure P4VP (162 °C) and P2VP (78 °C) homopolymers each exhibited only a single T_g value. For PS-*b*-PVPh/P4VP blends, as displayed in Fig. 2(a), we observed two values of T_g at all blend compositions, indicating that microphase separation may occur in this blend system; the lower value of T_g (106–126 °C) corresponded to the PS domain, while the higher value (194–208 °C) represented the hydrogen-bonded PVPh/P4VP miscible domain. Interestingly, the values of T_g of the PVPh/P4VP miscible domain were higher than those of the individual homopolymers at all blend compositions, presumably because of strong hydrogen bonding interactions, and also higher than those of the binary PVPh/P4VP homopolymer blend obtained from DMF solutions (the highest value of T_g was 190 °C at the molar ratio of 1 : 1),[65] presumably because of the nano-confinement of the block copolymer segments from the microphase separation. Therefore, the chain mobility of the PVPh/P4VP miscible phase in the PS-*b*-PVPh/P4VP system was relatively restricted and resulted in the formation of ordered nanostructures with more compact packing and a relatively smaller free volume, corresponding to higher values of T_g. Fig. 2(b) displays DSC heating scans of the PS-*b*-PVPh/P2VP blends. Again, we observed two values of T_g at P2VP compositions of less than 70 wt%; the lower value (100–106 °C) corresponded to that of the PS domain, while the higher value (121–190 °C) represented the hydrogen-bonded PVPh/P2VP miscible domain. A single value of T_g existed for PS-*b*-PVPh/P2VP = 20/80, because the PVPh/P2VP miscible phase was depressed to the same temperature range of the PS domain coincidence. Further increasing the P2VP content to PS-*b*-PVPh/P2VP = 10/90 led to the two values

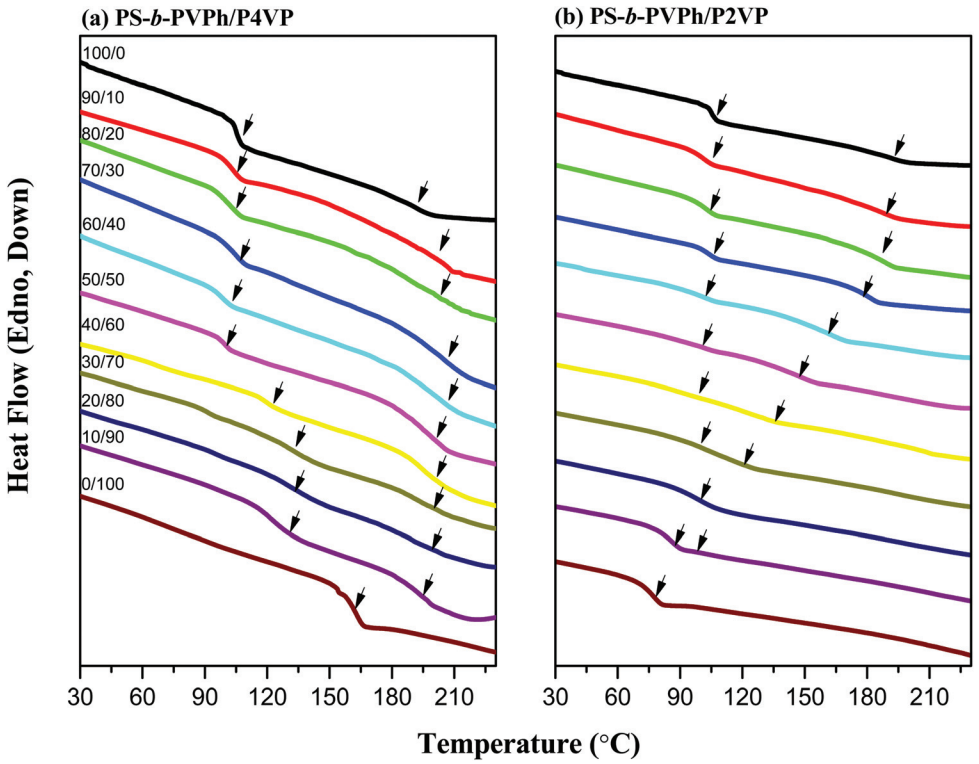

Fig. 2 DSC thermal analyses of (a) PS-*b*-PVPh/P4VP and (b) PS-*b*-PVPh/P2VP blends at various P4VP and P2VP concentrations.

of T_g appearing again; the lower (87 °C) represented miscible PVPh/P2VP, while the higher (100 °C) corresponded to the PS domain. All of the DSC results confirmed that microphase separation was occurring in this blend. Nevertheless, the T_g value of the PVPh/P2VP miscible domain was decreased upon increasing the P2VP concentration—in contrast to the PVPh/P4VP miscible domain behavior, where the values were higher than those of the individual homopolymers at all blend compositions.

Fig. 3 summarizes the T_g behavior for PS-*b*-PVPh/P4VP and PS-*b*-PVPh/P2VP blends. The values of T_g of the PVPh/P4VP and PVPh/P2VP domains both exhibited positive deviations based on the linear rule (green line in Fig. 3). The Kwei equation (red line in Fig. 3) was generally used to predict the glass transition temperatures of hydrogen-bonded blend systems:[66]

$$T_g = \frac{W_1 T_{g1} + kW_2 T_{g2}}{W_1 + kW_2} + qW_1 W_2 \quad (1)$$

where T_{gi} corresponds to the glass transition temperature of each component; W_i is each component's weight fraction; k and q are the fitting constants that describe the hydrogen bonding strength. From the Kwei equation we can obtain k and q values of 1 and 110, respectively, for the PS-*b*-PVPh/P4VP blend, which is similar to those for most P4VP blend systems featuring hydrogen bonding, and the values of 1 and 40, respectively, for the PS-*b*-PVPh/P2VP blend. These positive q values indicate that inter-association hydrogen bonding (OH···pyridine) in PVPh/P4VP and PVPh/P2VP blends was strong relative to self-association hydrogen bonding (OH···OH) of the PVPh segment. In addition, the positive q value for the PVPh/P4VP blend was higher than that for the PVPh/P2VP blend because the greater steric hindrance of P2VP affected its intermolecular interactions.[53,54,67] The difference in hydrogen bonding strength was consistent with the values of K_A based on PCAM, whereas that of PVPh/P4VP (K_A = 1200) was higher than that of PVPh/P2VP (K_A = 598),[52] which may affect the self-assembly structure and is investigated in the following section.

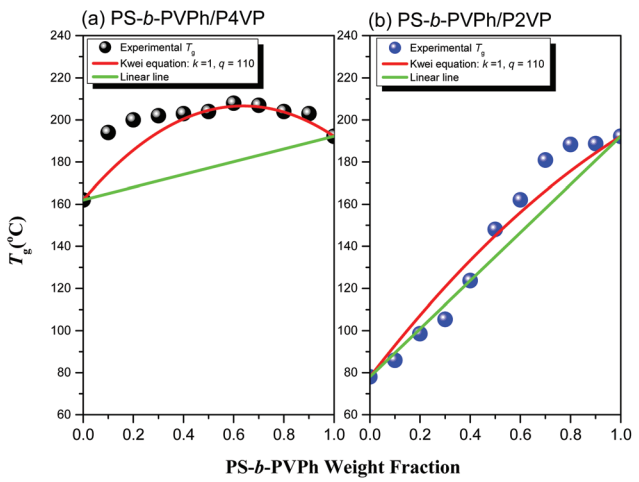

Fig. 3 Experimental and predicted (Kwei equation) values of T_g of (a) PVPh/P4VP and (b) PVPh/P2VP miscible domains.

Self-assembled structures in PS-*b*-PVPh/P4VP and PS-*b*-PVPh/P2VP blend systems

Fig. 4(a) displays the SAXS profile of the pure PS-*b*-PVPh diblock copolymer (f_v^{ps} = 0.67) at room temperature, revealing the long-range order of a lamellar structure with relative positions of 1 : 2 : 3 : 4. The first SAXS peak position at a q value of 0.209 nm^{-1} indicates a long period of 30.04 nm ($2\pi/q$) for this lamellar structure. The TEM image in Fig. 4(i) of the pure PS-*b*-PVPh reveals an alternative lamellar structure with the lamellar period of *ca.* 30 nm, which is consistent with the SAXS analysis in Fig. 4(a). This result is similar to a previous study where the PS volume fraction is f_v^{ps} = 0.63.[24] We observed more higher-order peaks at a 20 wt% content of P4VP, as revealed in Fig. 4(b), compared with the pure PS-*b*-PVPh diblock copolymer; the relative positions of 1 : 2 : 3 : 4 : 5 were indicative of a long-range-ordered lamellae structure, as confirmed by the TEM image in Fig. 4(j). Furthermore, the first-order peak had shifted slightly to the higher-q region at a 20 wt% content of P4VP (q_{max} = 0.211 nm^{-1}; d-spacing = 29.76 nm), revealing shrinkage of the inter-lamellar spacing D, consistent with the theoretical prediction.[25] Using the interpolymer complexation model (ICM), Shi *et al.* proposed that the increase in the concentration of a strongly hydrogen bonding homopolymer in the presence of a diblock copolymer would result in a decrease in the lamellar spacing.[25] The interpolymer complex formed with the homopolymer P4VP would increase the effective volume fraction and the interfacial area of the PVPh segment in the block copolymer and, thus, the PS chain should occupy the same volume as that prior to complexation; therefore, the PS domain should shrink and drive this system into an order–order morphological transition. Interestingly, an order–order transition from the lamellar to bicontinuous gyroid structure occurred upon increasing the P4VP concentration to 30 wt%. The maximum peak appeared at a value of $\sqrt{6}q^*$ of 0.231 nm^{-1} (d = 27.18 nm) with the most ordered peaks at $\sqrt{8} : \sqrt{14} : \sqrt{16} : \sqrt{20} : \sqrt{46}$ [see the inset in Fig. 4(c)], indicating the long-range order of the bicontinuous gyroid structure, as confirmed by the TEM image in Fig. 4(k) from the [111] direction. This bicontinuous gyroid structure had also been observed by Chen *et al.* in the study of a PS_{107}-*b*-$PVPh_{63}$/$P4VP_{52}$ = 60/40 blend system, although the molecular weights of the diblock copolymer and the homopolymer were different from those in the present study. Further increases in the P4VP concentration to 40 or 50 wt% resulted in the SAXS patterns [Fig. 4(d) and (e)] displaying the long-range order of cylindrical structures with peak ratios of $1 : \sqrt{3} : \sqrt{4} : \sqrt{7} : \sqrt{12}$, as confirmed in TEM images [Fig. 4(l) and (m)]. The maximum peaks appeared at q^* values of 0.175 nm^{-1} (d = 35.88 nm) for 40 wt% P4VP and 0.197 nm^{-1} (d = 31.87 nm) for 50 wt% P4VP. When the P4VP concentrations were 60, 70, and 90 wt%, the SAXS patterns [Fig. 4(g) and (h)] exhibited peak ratios of $1 : \sqrt{3} : \sqrt{7}$ and the TEM images [Fig. 4(n)–(p)] revealed that these samples possessed spherical structures. Clearly, the addition

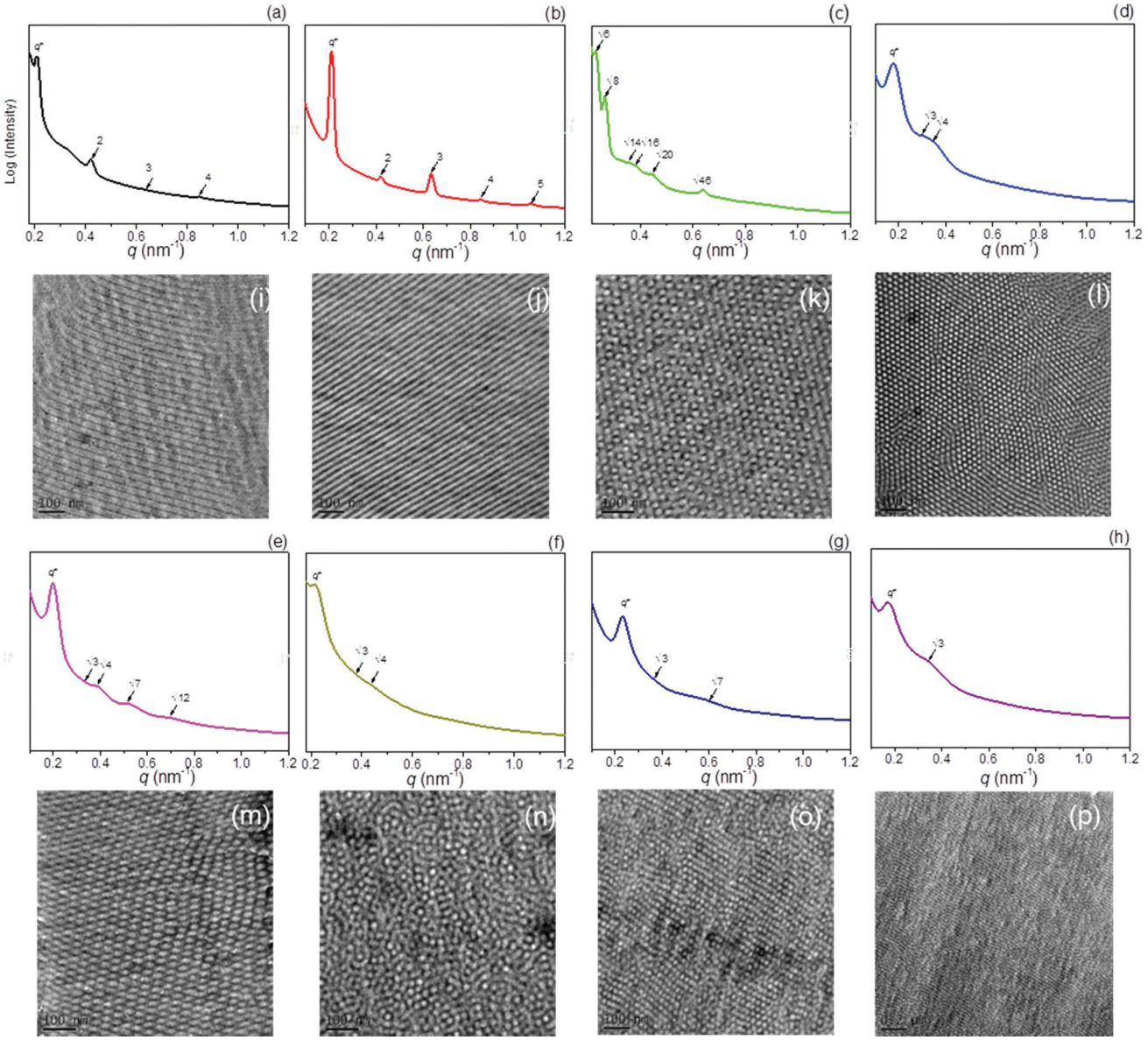

Fig. 4 SAXS analyses and TEM images of (a, i) pure PS-*b*-PVPh and (b)–(h) PS-*b*-PVPh/P4VP blends at P4VP concentrations of (b, j) 20, (c, k) 30, (d, l) 40, (e, m) 50, (f, n) 60, (g, o) 70, and (h, p) 90 wt%.

of the homopolymer P4VP induced a sequence of order–order transitions from lamellae to bicontinuous gyroids to hexagonally packed cylinders and, finally, to sphere structures.

Next, we turned our attention to the self-assembled structures in the PS-*b*-PVPh/P2VP blend system (Fig. 5). Similar to the P4VP blend system, the SAXS pattern recorded at 20 wt% P2VP [Fig. 5(b)] also exhibited long-range order of the lamellae structure with relative positions of 1 : 2 : 3 : 4, as confirmed using TEM [Fig. 5(j)]. Furthermore, the first peak also shifted to the higher-q region at 20 wt% P2VP (q_{max} = 0.232 nm^{-1}; d-spacing = 27.06 nm), revealing shrinkage of the inter-lamellar spacing D, similar to the phenomenon that occurred for the P4VP blend system. Increasing the P2VP concentration to 30 wt% retained the long-range order of a lamellae structure with peaks at 1 : 3 : 5, confirmed by TEM imaging [Fig. 5(k)]. Here, the even-order peaks disappeared because the value of f_v^{ps} was 0.48 at this blend composition. The intensity of the n^{th}-order peak for a lamellae structure is proportional to $\sin^2(\pi n\Phi_a)/n^2$, when Φ_a (volume fraction of the A segment) is close to 0.5, the even-order intensities (peaks 2 and 4) were depressed to zero height.[68] This result differs from that of the PS-*b*-PVPh/P4VP = 70/30 blend which exhibited a bicontinuous gyroid structure. Further increasing the P2VP concentration to 40–60 wt%, the SAXS patterns [Fig. 5(d)–(f)] also revealed the long-range order of cylindrical structures with peak ratios of $1 : \sqrt{3} : \sqrt{4} : \sqrt{7} : \sqrt{9}\sqrt{12}$, consistent with TEM images [Fig. 5(l)–(n)]. The maximum peaks appeared at q^* values of 0.181 nm^{-1} (d = 34.69 nm) for 40 wt% P2VP, 0.180 nm^{-1}

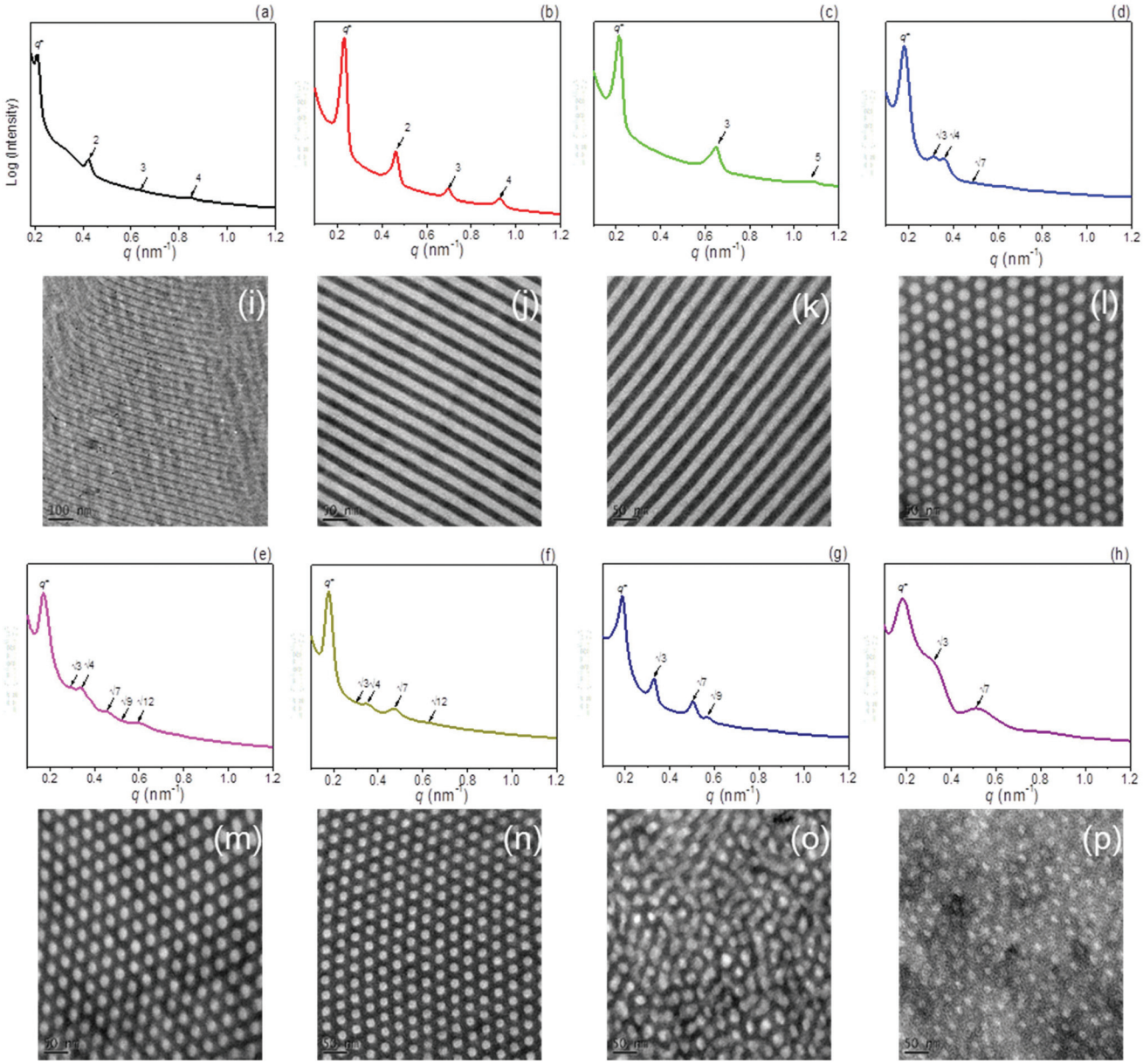

Fig. 5 SAXS analyses and TEM images of (a, i) pure PS-*b*-PVPh and (b)–(h) PS-*b*-PVPh/P2VP blends at P2VP concentrations of (b, j) 20, (c, k) 30, (d, l) 40, (e, m) 50, (f, n) 60, (g, o) 70, and (h, p) 90 wt%.

(d = 34.88 nm) for 50 wt% P2VP, and 0.179 nm^{-1} (d = 35.08 nm) for 60 wt% P2VP. Similar to the P4VP blend systems at 40–60 wt%, the P2VP blend systems also showed the long-range order of cylindrical structures. Further increasing the P2VP concentrations to 70 and 90 wt%, the SAXS patterns [Fig. 5(g) and (h)] exhibited peak ratios of $1:\sqrt{3}:\sqrt{7}:\sqrt{9}$; TEM imaging [Fig. 5(o) and (p)] revealed a spherical structure at 70 wt% P2VP and a disordered spherical micelle structure at 90 wt% P2VP. Thus, once again, the addition of the homopolymer P2VP induced a sequence of order–order transitions from lamellae to hexagonally packed cylinders to, finally, sphere structures. The order–order morphological transitions in these PS-*b*-PVPh/P4VP and PS-*b*-PVPh/P2VP blends were driven by the effective interaction parameters increasing through strong hydrogen bonding interaction in PVPh/P4VP and PVPh/P2VP domains, thereby changing the volume fractions in the microphase-separated block segments. The only morphological difference in these two blend systems was that a bicontinuous gyroid structure formed in the PS-*b*-PVPh/P4VP blend, but not in the PS-*b*-PVPh/P2VP blend system. Bicontinuous gyroid structures exist only in very narrow regions between lamellae and cylindrical structures with low values of χN, based on the diblock copolymer phase diagram derived from mean field theory.[69] Nevertheless, when we attempted to expand the P2VP concentrations between 30 and 40 wt% (*i.e.*, 32, 34, 36, and 38 wt%) we observed only the lamellae and cylindrical structures in SAXS analyses (Fig. S1†).

In other words, we did not observe any bicontinuous gyroid structures for the PS-*b*-PVPh/P2VP blend system. Because we used the same diblock copolymer in these two blend systems and the molecular weights of P4VP and P2VP were similar, the volume fractions and degrees of polymerization (N) were almost identical for the same at 30 wt% P4VP and P2VP. In addition, the solubility parameters of the homopolymers P4VP and P2VP were also the same, as determined using the group contribution method, due to these two homopolymers being isomers.[49] The only difference between them was their different strengths of hydrogen bonding, arising from steric effects, thereby inducing different values of χ and K_A. In addition, simulations suggest that a relatively low hydrogen bonding strength (low values of χ or K_A) would require the addition of more of the homopolymer to induce the order–order transition and display macrophase separation. This behavior is consistent with our experimental finding that 30 wt% P4VP already transformed the system into a bicontinuous gyroid structure, whereas the system containing 30 wt% P2VP retained its lamellae structure; 60 wt% P4VP transformed the system to spheres, whereas the system containing 60 wt% P2VP retained its cylindrical structure; and 90 wt% P4VP transformed the system to spheres, whereas the system containing 90 wt% P2VP exhibited macrophase separation.

FTIR spectroscopic analysis of PS-*b*-PVPh/P4VP and PS-*b*-PVPh/P2VP blend systems

FTIR spectroscopy analysis is a highly effective method for characterizing the intermolecular hydrogen bonding strength. Fig. 6 displays the FTIR spectral region of the pyridine groups for PS-*b*-PVPh/P4VP and PS-*b*-PVPh/P2VP blends. The P4VP and P2VP homopolymers usually exhibit absorption for free pyridyl groups near 993 cm^{-1}; a new band representing hydrogen bonded pyridine units with the PVPh block segment appeared near 1003 cm^{-1}. In addition, pure PVPh provided the absorption band near 1013 cm^{-1}. We used digital subtraction of the signal near 1013 cm^{-1} by considering the molar fraction of the PVPh segment in the blend system, as displayed in Fig. S1,† where only two bands (free and hydrogen bonded pyridine) were present that could be resolved well by the Gaussian function.[62] The hydrogen-bonded pyridyl unit fraction of both P4VP and P2VP increased upon increasing the PS-*b*-PVPh diblock copolymer concentration. Fig. 7 summarizes the fraction of hydrogen-bonded pyridine groups obtained *via* curve-fitting of the results in Fig. S2.† The fraction of hydrogen-bonded pyridine groups of P4VP was always higher than that of P2VP for all blend compositions, presumably because of the steric effects of these two homopolymers, consistent with the DSC and PCAM results. At relatively low P4VP and P2VP concentrations, the higher fraction of hydrogen-bonded pyridine units of P4VP induced long-range-ordered self-assembled structures from lamellae to bicontinuous gyroids to hexagonally packed cylinders and, finally, to sphere structures without macrophase separation. In contrast, disordered spheres were observed at a high P2VP concentration (90 wt%) because the lower fraction of hydrogen bonding interaction (only 17.3%) induced macrophase separation, as would be expected.

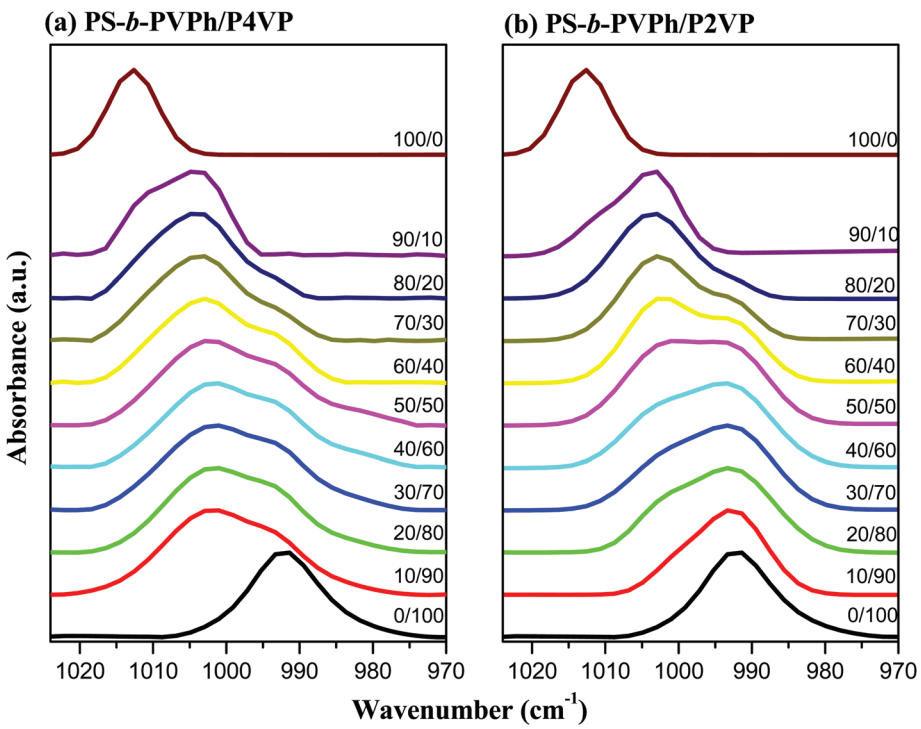

Fig. 6 FTIR spectra (recorded at room temperature) of (a) PS-*b*-PVPh/P4VP and (b) PS-*b*-PVPh/P2VP blends.

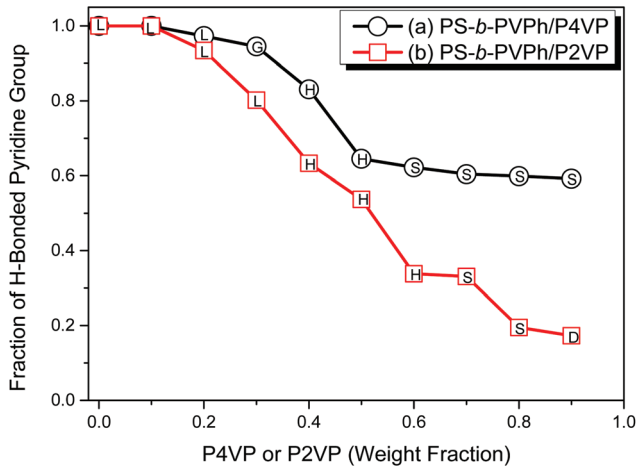

Fig. 7 Fractions of hydrogen-bonded pyridine groups of (a) PS-*b*-PVPh/P4VP and (b) PS-*b*-PVPh/P2VP blends at various homopolymer concentrations.

Self-assembled structures formed from PS-*b*-PVPh/P4VP and PS-*b*-PVPh/P2VP blend systems at various temperatures

Because the strength of hydrogen bonding is sensitive to the temperature,[70] we examined the types of self-assembled structures formed from the PS-*b*-PVPh/P4VP and PS-*b*-PVPh/P2VP blends at various temperatures. In general, the hydrogen bonding strength or value of K_A is weakened by an increase in temperature (van't Hoff equation); a blend system featuring such weaker hydrogen bonds may, therefore, undergo an order–order morphological transition upon increasing the temperature. Fig. S3† presents SAXS profiles of PS-*b*-PVPh/P4VP and PS-*b*-PVPh/P2VP = 30/70 blends recorded at various temperatures. Both blend systems had spherical structures at room temperature. The SAXS pattern of the PS-*b*-PVPh/P4VP = 30/70 blend [Fig. S3(a)†] did not change upon increasing the temperature (*i.e.*, it retained its spherical structure). In contrast, the SAXS patterns of the PS-*b*-PVPh/P2VP = 30/70 blend [Fig. S3(b)†] underwent obvious changes upon increasing the temperature, with the spherical structure transforming into a cylindrical structure with peak ratios of $1:\sqrt{3}:\sqrt{4}:\sqrt{7}:\sqrt{9}$ at temperatures higher than 120 °C. Fig. S4† also displays SAXS profiles of PS-*b*-PVPh/P4VP = 70/30 and PS-*b*-PVPh/P2VP = 60/40 blends recorded at various temperatures. The SAXS profiles of PS-*b*-PVPh/P4VP = 70/30 [Fig. S4(a)†] are similar to those of the PS-*b*-PVPh/P4VP = 30/70 blend system; they did not change upon increasing the temperature, suggesting that this blend system also had a bicontinuous gyroid structure at each temperature. In contrast, the SAXS patterns of the PS-*b*-PVPh/P2VP = 60/40 blend [Fig. S4(b)†] underwent an obvious change upon increasing the temperature: the cylindrical structure transformed into lamellae with peak ratios of 1 : 2 : 3 : 4 : 5. To prove that the PS-*b*-PVPh/P2VP = 60/40 blend experienced a morphological order–order transition upon increasing the temperature, we maintained the TEM samples at the elevated temperature for 1 day and then quickly quenched them to room temperature, using liquid N_2, to maintain the high temperature morphology. Fig. 8 reveals the clear morphological order–order transition of the PS-*b*-PVPh/P2VP = 60/40 blend at various temperatures, based on SAXS and TEM analyses. Fig. 8(a) displays the long-range order of cylindrical structures having a peak ratio of $1:\sqrt{3}:\sqrt{4}:\sqrt{7}$, consistent with the TEM image in Fig. 8(d). Further increasing the temperature to 120 and 140 °C, the SAXS patterns change to the long-range order of lamellae structures with a peak ratio of 1 : 2 : 3 : 4 : 5 : 6 [Fig. 8(b) and (c), respectively]. TEM imaging confirmed the large area and long-range order of the lamellae structures [Fig. 8(e) and (f)].

These results reveal that the self-assembled structures formed from relatively weakly hydrogen bonding blend systems can change upon increasing the temperature. For confirmation, we recorded FTIR spectra at various temperatures to examine the strength of the hydrogen bonding in these two blend systems (Fig. 9). In both blend systems, the fraction of hydrogen-bonded pyridine units (signal at 1003 cm^{-1}) as mentioned above was decreased upon increasing the temperature. Based on the van't Hoff equation ($K = -\Delta h/RT + C$), we plotted the equilibrium constants with respect to temperature, using the values of K_A that were used for PVPh/P4VP and PVPh/P2VP of 1200 and 598, respectively, at 25 °C and a value of K_B for pure PVPh of 66.8. In addition, the enthalpy of hydrogen bonding for PVPh/P4VP and PVPh/P2VP (h_A) in this study was −7.0 kcal mol^{-1}, while the enthalpy of hydrogen bonding for pure PVPh (h_B) was −5.2 kcal mol^{-1}. Fig. 10(a) displays the change in equilibrium constant with respect to temperature at different rates; the difference in the values of K_A and K_B decreased at relatively high temperatures.[71] This predicted curve is close to that of the hydrogen-bonded pyridine fractions, which decreased from 0.604 to 0.241 for the PS-*b*-PVPh/P4VP = 30/70 and from 0.331 to 0.143 for the PS-*b*-PVPh/P2VP = 30/70 blend compositions [Fig. 10(b)]. The difference in the fraction of hydrogen-bonded pyridine units was 0.273 at 25 °C and 0.098 at 200 °C. Furthermore, the fraction of hydrogen-bonded pyridine units in the PS-*b*-PVPh/P4VP blend was always higher than that in the PS-*b*-PVPh/P2VP blend at the same homopolymer content. PS-*b*-PVPh/P4VP, with its stronger hydrogen bonding, did not undergo a morphological change, but PS-*b*-PVPh/P2VP, with its relatively weaker hydrogen bonding, did upon increasing the temperature. Another possibility is that the T_g of the PS-*b*-PVPh/P4VP blend (*ca.* 200 °C) is higher than that of the PS-*b*-PVPh/P2VP blend and there is a possibility that the transition is prohibited by the vitrification even though the cylinder structure is thermodynamically stable at higher temperature in strong hydrogen bonding of the PS-*b*-PVPh/P4VP blend.

Effect of hydrogen bonding strength on self-assembled structures

In this section, we summarize the effects of the different hydrogen bonding strengths on the self-assembled structures formed in A-*b*-B/C blends, including PS-*b*-PVPh/P4VP (K_A = 1200), PS-*b*-PVPh/P2VP (K_A = 598), and PS-*b*-PVPh/PMMA (K_A =

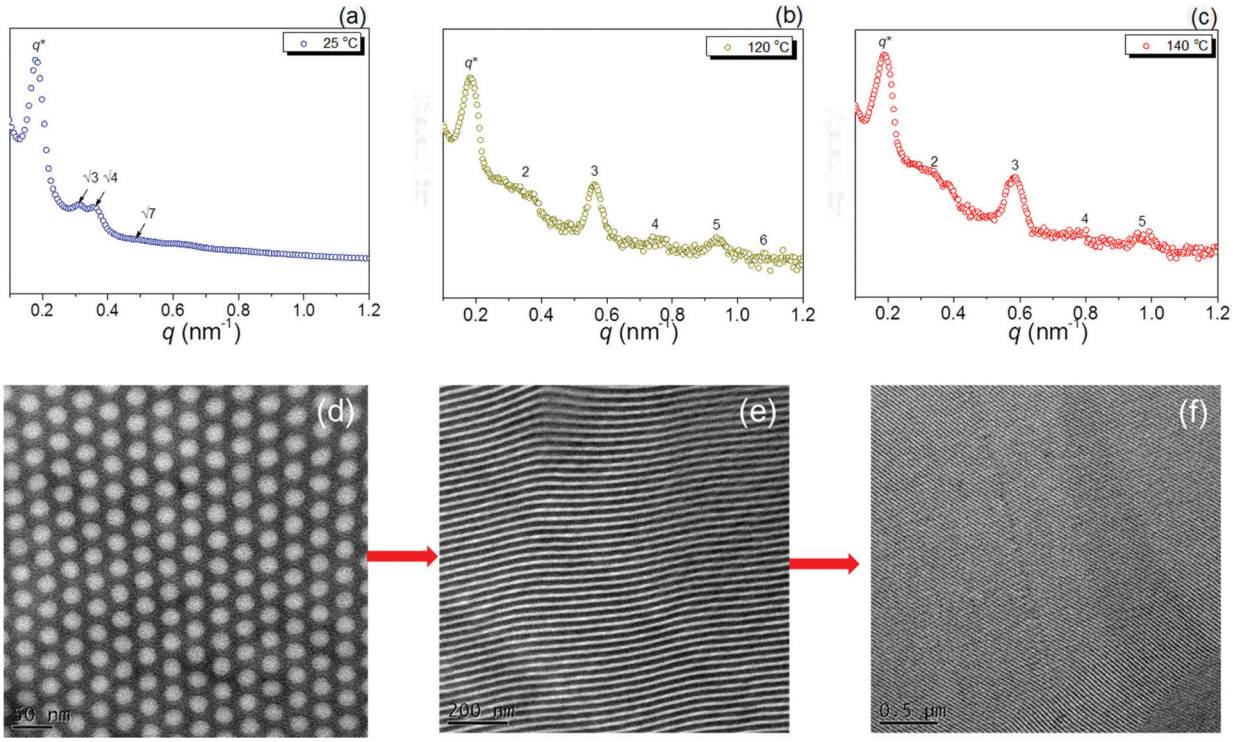

Fig. 8 SAXS analyses and TEM images of the PS-*b*-PVPh/P2VP = 60/40 blend recorded at temperatures of (a, d) 25, (b, e) 120, and (c, f) 140 °C.

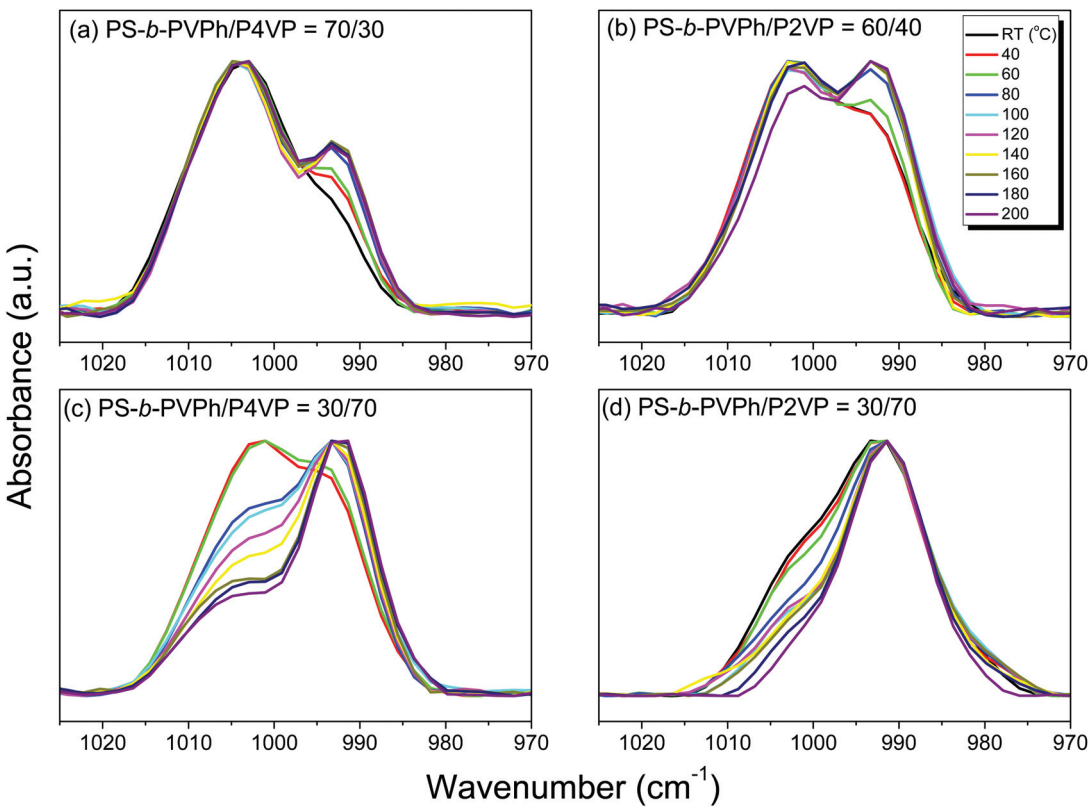

Fig. 9 FTIR spectra (recorded at various temperatures) of (a) PS-*b*-PVPh/P4VP = 70/30, (b) PS-*b*-PVPh/P2VP = 60/40, (c) PS-*b*-PVPh/P4VP = 30/70, and (d) PS-*b*-PVPh/P2VP = 30/70 blends.

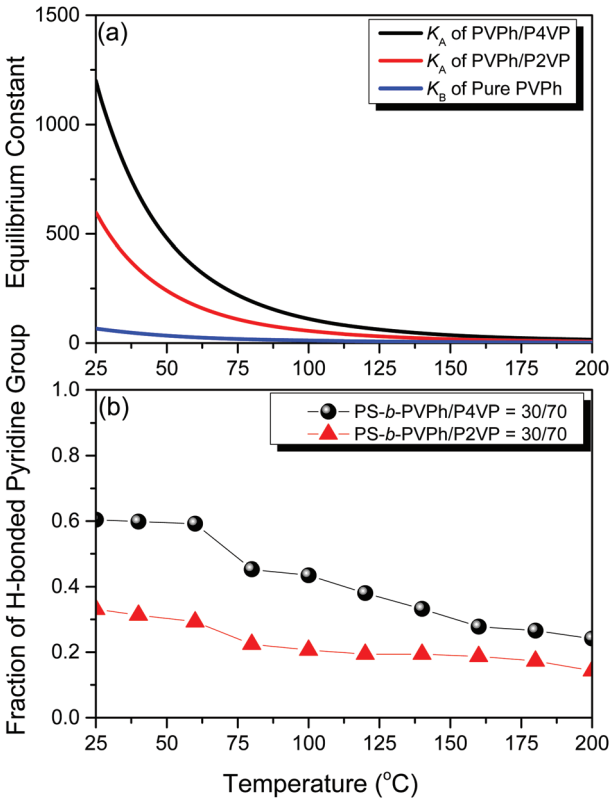

Fig. 10 (a) Equilibrium constants and (b) fractions of hydrogen-bonded pyridine groups for PS-*b*-PVPh/P4VP and PS-*b*-PVPh/P2VP blends plotted with respect to temperature.

37.4). Fig. 11 presents phase diagrams of the PS-*b*-PVPh/P4VP, PS-*b*-PVPh/P2VP, and PS-*b*-PVPh/PMMA blends.[24] The system with the weakest hydrogen bonds, PS-*b*-PVPh/PMMA, exhibited only the lamellae structure at lower PMMA concentrations (<40 wt% or f_{ps}^{v} = 0.43–0.61), but it displayed undulated lamellae or macrophase separation at higher PMMA concentrations (>40 wt% or f_{ps}^{v} = 0.06–0.43); thus, it exhibited dry-brush behavior.[24] In contrast, the PS-*b*-PVPh/P2VP blend, with its relatively strong hydrogen bonds, underwent a sequence of order–order transitions from lamellae to hexagonally packed cylinders to, finally, BCC spheres; that is, it displayed wet-brush behavior. This system possessed a lamellae structure at low P2VP concentrations (<34 wt% or f_{ps}^{v} = 0.44–0.66), transformed to hexagonally packed cylinders at moderate P2VP concentrations (34–70 wt% or f_{ps}^{v} = 0.21–0.44), transformed to spheres at high P2VP concentrations (70–80 wt% or f_{ps}^{v} = 0.14–0.21), and finally transformed to a disordered structure at the highest P2VP concentration (90 wt% or f_{ps}^{v} = 0.07). Most interestingly, the PS-*b*-PVPh/P4VP blend, which had the strongest hydrogen bonds, exhibited a full sequence of order–order transitions from lamellae, to bicontinuous gyroids, to hexagonally packed cylinders, and, finally, to BCC spheres; it also displayed wet-brush behavior. The lamellae structure of the pure PS-*b*-PVPh diblock copolymer readily transformed into the bicontinuous gyroid structure upon blending with P4VP at relatively low concentrations (30–40 wt% or f_{ps}^{v} = 0.41–0.48); such a bicontinuous gyroid structure was not observed upon blending with P2VP, PMMA, or PVPh homopolymers. In addition, PS-*b*-PVPh/P4VP, with its strongest hydrogen bonds, required the lowest homopolymer concentration (30 wt% or f_{ps}^{v} = 0.48) to induce the order–order transition; a relatively high homopolymer concentration was necessary to induce the order–order transition in the more weakly hydrogen bonding P2VP blend system (34 wt% or f_{ps}^{v} = 0.44). In contrast, the PS-*b*-PVPh/PMMA blend system, which had the weakest hydrogen bonds, already underwent its disordered and macrophase separation at a low homopolymer concentration (30 wt% or f_{ps}^{v} = 0.43). Increasing the P4VP concentration to a moderate level (40–60 wt% or f_{ps}^{v} = 0.28–0.41) transformed the PS-*b*-PVPh/P4VP system into hexagonally packed cylinders; finally, it transformed into BCC spheres upon further increasing the P4VP concentration (60–90 wt% or f_{ps}^{v} = 0.06–0.28). Comparing the PS-*b*-PVPh/P4VP and PS-*b*-PVPh/P2VP blend systems, the former already transformed into BCC spheres at 60 wt% P4VP and did not display macrophase separation at higher P4VP concentrations (90 wt%); in contrast, the latter transformed into BCC spheres at 70 wt% P2VP and displayed macrophase separation at 90 wt% P2VP. These results were predicted well using the theoretical approach described by the Shi group.[25] The A-*b*-B/C system featuring the strongest hydrogen bonds readily underwent the order–order morphological transitions at lower homopolymer concentrations and did not form a two-phase region at higher homopolymer concentrations.

In addition, we investigated the homopolymer distributions in these three blend systems. From the average distance of the chemical junction for a diblock copolymer interface (a_J), the relative change (a_J/a_{J_0}) could be calculated after the addition of a homopolymer, where a_{J_0} represents the value for the pure block copolymer in the absence of blending. The following formulae were used based on a simple volumetric conversion: for a lamellar structure, $D/D_0 = (\rho_J/\rho_{J_0})/\Phi_{block}$; for a cylindrical structure, $D/D_0 = (\rho_J/\rho_{J_0})[(2/3^{1/2})\pi(1-f)/\Phi_{block}]^{1/2}$; and for a BCC spherical structure, $D/D_0 = (\rho_J/\rho_{J_0})[(27\sqrt{3}/8)\pi(1-f)^2/\Phi_{block}]^{1/2}$.[12,13] Here, f is the PS volume fraction, D_0 is the pure diblock copolymer interdistance, Φ is the block copolymer volume fraction in the blend system, and ρ_J is the number of block chains per unit interfacial area (a_J^2); in this case, we obtain the formula $a_J/a_{J_0} = (\rho_J/\rho_{J_0})^{-1/2}$. Fig. 12 displays the values of a_J/a_{J_0} obtained from the equations above for PS-*b*-PVPh/P4VP, PS-*b*-PVPh/P2VP, and PS-*b*-PVPh/PMMA blends at various homopolymer concentrations. The values of a_J for all three blends increased upon increasing the homopolymer concentration ($a_J/a_{J_0} > 1$); these three blends all exhibited lamellae structures with lower a_J/a_{J_0} values at relatively low homopolymer concentrations. The PS-*b*-PVPh/PMMA blend, with its weakest hydrogen bonds, displayed the lamellae structure only at PMMA concentrations of less than 40 wt%; its value of a_J/a_{J_0} was the lowest among all three systems. It transformed into a disordered undulated lamellae structure at PMMA concentrations greater than 40 wt%.[24] The PS-*b*-PVPh/P4VP and PS-*b*-PVPh/P2VP blends, which

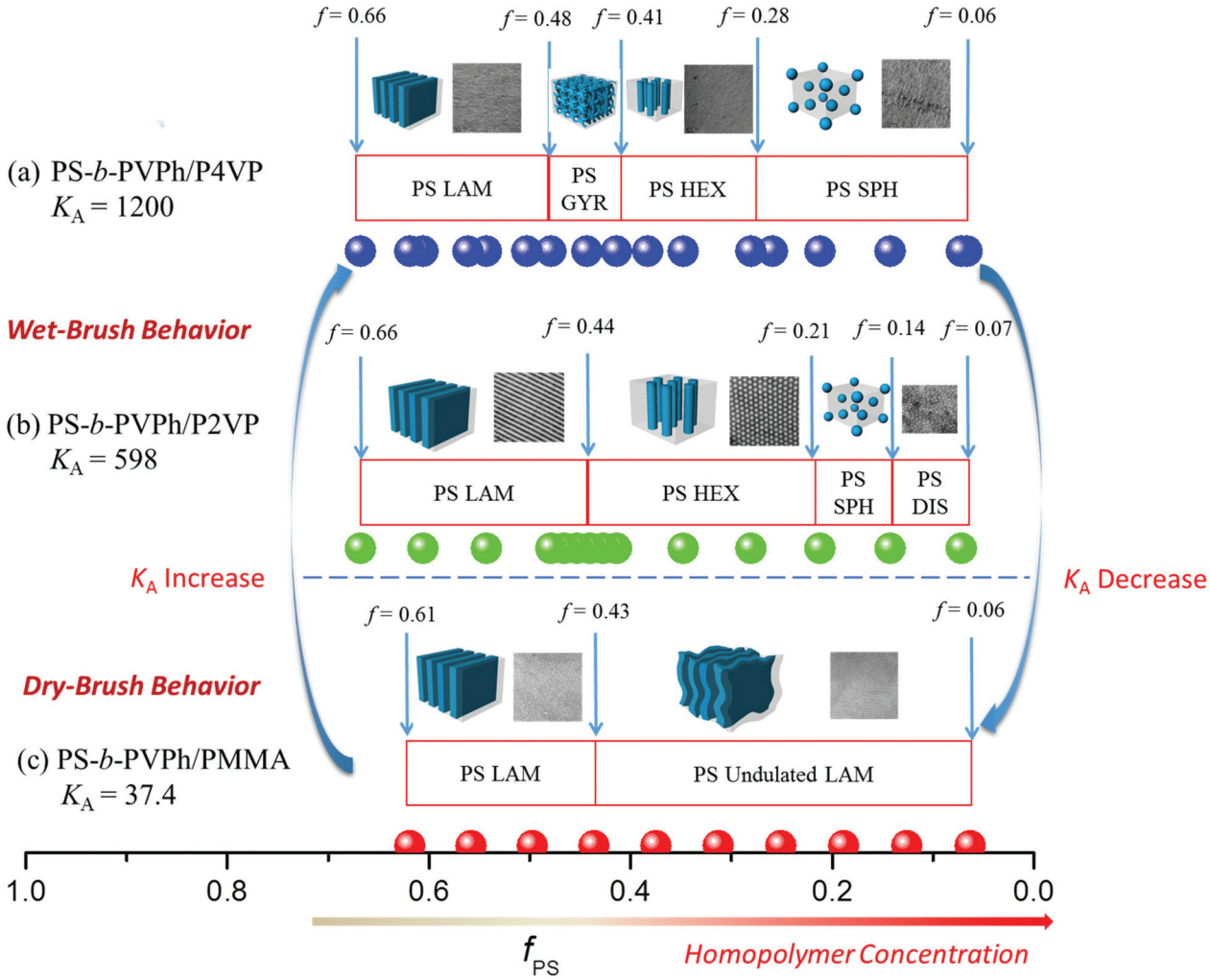

Fig. 11 Phase diagrams and experimental PS volume fractions of (a) PS-*b*-PVPh/P4VP, (b) PS-*b*-PVPh/P2VP, and (c) PS-*b*-PVPh/PMMA blends.[24]

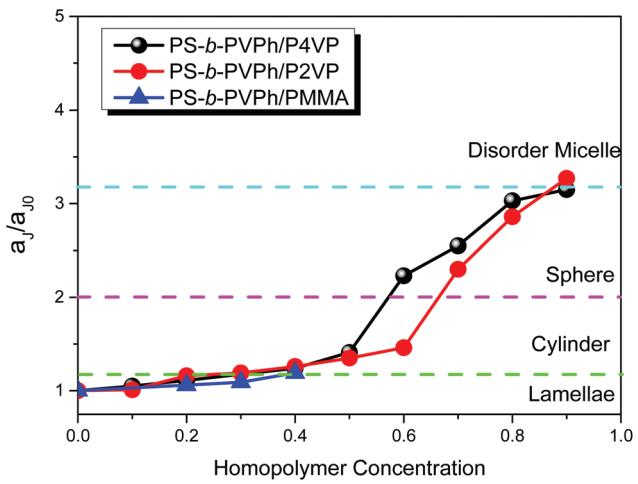

Fig. 12 Values of a_J/a_{J_0} for (a) PS-*b*-PVPh/P4VP, (b) PS-*b*-PVPh/P2VP, and (c) PS-*b*-PVPh/PMMA blends.[24]

featured strong hydrogen bonds, exhibited wet-brush behavior upon increasing the P4VP and P2VP concentrations. At relatively low P2VP concentrations (*ca.* 10–30 wt%), these blends all exhibited the lamellae structure with lower values of a_J/a_{J_0} (<1.19). When the P2VP concentration increased to 40–60 wt%, an order–order morphological transition behavior occurred from lamellae to a hexagonally packed cylinder structure, with higher values of a_J/a_{J_0} (1.26–1.46), consistent with the volume fraction of the block copolymer segment changing as a result of the strong hydrogen bonding of the PVPh/P2VP miscible domain. Further increasing the P2VP concentration to 70–90 wt% caused the self-assembled structure to transform into BCC spheres (70–80 wt%) and disordered spheres (90 wt%), respectively, with values of a_J/a_{J_0} of 2.30–3.27. In addition, the blend also possessed a lamellae structure with lower values of a_J/a_{J_0} (<1.11) at relatively low P4VP concentrations (*ca.* 10–20 wt%); it transformed into a bicontinuous gyroid structure at 30 wt% P4VP; it then transformed into the hexagonally packed cylinders at 40–50 wt% P4VP with higher values of a_J/a_{J_0} of 1.24–1.41; finally, it transformed into the BCC spheres at

60–90 wt% P4VP with values of a_J/a_{J_0} of 2.23–3.15. Because the hydrogen bonding of P4VP was stronger than that of P2VP, the former possessed higher values of a_J/a_{J_0}, suggesting that the P4VP homopolymer dissolved into the PVPh segment, readily swelling the inter-distance of the chemical junction for the diblock copolymer interface. Similarly, the A-*b*-B/C system with the strongest hydrogen bonding readily exhibited its order–order morphological transition at a lower homopolymer concentration and did not exhibit a two-phase region at higher homopolymer concentrations; this behavior can be understood by considering that the value of a_J/a_{J_0} at 90 wt% P2VP was higher than that at 90 wt% P4VP, because the macrophase had already occurred in the P2VP blend system. In summary, the different degrees of steric hindrance of P4VP and P2VP resulted in different hydrogen bonding strengths in PS-*b*-PVPh diblock copolymer blends and did, indeed, affect the resulting self-assembled structures.

Conclusions

We have used DSC, SAXS, TEM, and FTIR spectroscopy to study the thermal properties, hydrogen bonding interactions, and self-assembled structures of PS-*b*-PVPh/P4VP and PS-*b*-PVPh/P2VP blends. The self-assembled structures of these A-*b*-B/C systems were strongly dependent on the strength of the hydrogen bonding, influenced by steric effects, of the homopolymers P4VP and P2VP. The PS-*b*-PVPh/P2VP blend, which had relatively weak hydrogen bonds, exhibited an incomplete sequence of order–order morphological transitions from lamellae, to hexagonally packed cylinders, to BCC spherical structures upon increasing the P2VP concentration; it also formed disordered spheres at a relatively high P2VP concentration (90 wt%). In contrast, the PS-*b*-PVPh/P4VP blend, with its stronger hydrogen bonds, underwent the full sequence of order–order transitions from lamellae, to bicontinuous gyroids, to hexagonally packed cylinders, and, finally, to BCC spheres upon increasing the P4VP concentration; it did not form disordered spheres at relatively high P4VP concentrations. Although the hydrogen bonding in the PS-*b*-PVPh/P2VP blends was weaker than that in the PS-*b*-PVPh/P4VP blend, the former did exhibit wet-brush behavior, because its value of K_A was significantly higher than the value of K_B of PVPh; this situation is different from that of the PS-*b*-PVPh/PMMA blends, which displayed dry-brush behavior because of its even weaker hydrogen bonds. We conclude that the strength of hydrogen bonding is a key feature influencing the self-assembled structures formed in A-*b*-B/C systems.

Acknowledgements

This work was financially supported by the Ministry of Science and Technology, Taiwan, under contract MOST 102-2221-E-110-008-MY3. We also thank Mr Hsien-Tsan Lin of the Regional Instruments Center at National Sun Yat-Sen University for help with TEM experiments.

References

1 F. Yang, Z. Q. Cao and G. J. Wang, *Polym. Chem.*, 2015, **6**, 7995–8002.
2 K. W. Tan, D. T. Moore, M. Saliba, H. Sai, L. A. Estroff, T. Hanrath, H. J. Snaith and U. Wiesner, *ACS Nano*, 2014, **8**, 4730–4739.
3 A. H. Hofman, G. O. R. A. van Ekenstein, A. J. J. Woortman, G. ten Brinke and K. Loos, *Polym. Chem.*, 2015, **6**, 7015–7026.
4 C. A. Ross, K. K. Berggren, J. Y. Cheng, Y. S. Jung and J. B. Chang, *Adv. Mater.*, 2014, **26**, 4386–4396.
5 K. W. Tan, B. Jung, J. G. Werner, E. R. Rhoades, M. O. Thompson and U. Wiesner, *Science*, 2015, **349**, 54–58.
6 T. N. Hoheisel, K. Hur and U. B. Wiesner, *Prog. Polym. Sci.*, 2015, **40**, 3–32.
7 Y. Chen, K. Zhang, X. Wang, F. Zhang, J. Zhu, J. W. Mays, K. L. Wooley and D. J. Pochan, *Macromolecules*, 2015, **48**, 621–5631.
8 K. Yu and A. Eisenberg, *Macromolecules*, 1996, **29**, 6359–6361.
9 M. W. Matsen and F. S. Bates, *Macromolecules*, 1996, **29**, 7641–7644.
10 A. V. Dobrynin and I. Y. Erukhimovich, *Macromolecules*, 1993, **26**, 276–281.
11 A. K. Khandpur, S. Foerster, F. S. Bates, I. W. Hamley, A. J. Ryan, W. Bras, K. Almdal and K. Mortensen, *Macromolecules*, 1995, **28**, 8796–8806.
12 T. Hashimoto, H. Tanaka and H. Hasegawa, *Macromolecules*, 1990, **23**, 4378–4386.
13 T. Tanaka, H. Hasegawa and T. Hashimoto, *Macromolecules*, 1991, **24**, 240–251.
14 Y. K. Han, E. M. Pearce and T. K. Kwei, *Macromolecules*, 2000, **33**, 1321–1329.
15 M. Jiang and H. K. Xie, *Prog. Polym. Sci.*, 1991, **16**, 977–1026.
16 W. V. Zoelen, G. A. V. Ekenstein, O. Ikkala and G. Ten-Brinke, *Macromolecules*, 2006, **39**, 6574–6579.
17 Y. Y. Huang, J. Y. Hsu, H. L. Chen and T. Hashimoto, *Macromolecules*, 2007, **40**, 3700–3707.
18 J. Q. Zhao, E. M. Pearce and T. K. Kwei, *Macromolecules*, 1997, **30**, 7119–7126.
19 H. Kosonen, J. Ruokolainen, P. Nyholm and O. Ikkala, *Macromolecules*, 2001, **34**, 3046–3049.
20 Y. Matsushita, *Macromolecules*, 2007, **40**, 771–776.
21 K. Dobrosielska, S. Wakao, A. Takano and Y. Matsushita, *Macromolecules*, 2008, **41**, 7695–7698.
22 K. Dobrosielska, S. Wakao, J. Suzuki, K. Noda, A. Takano and Y. Matsushita, *Macromolecules*, 2009, **42**, 7098–7102.
23 S. W. Kuo, *Polym. Int.*, 2009, **58**, 455–464.

24 S. C. Chen, S. W. Kuo, U. S. Jeng, C. J. Su and F. C. Chang, *Macromolecules*, 2010, **43**, 1083–1092.
25 A. Dehghan and A. C. Shi, *Macromolecules*, 2013, **46**, 5796–5805.
26 N. Hameed and Q. Guo, *Polymer*, 2008, **49**, 5268–5275.
27 N. Hameed and Q. Guo, *Macromolecules*, 2008, **41**, 7596–7605.
28 N. Hameed, N. V. Salim and Q. Guo, *J. Chem. Phys.*, 2009, **131**, 214905.
29 N. V. Salim, T. Hanley and Q. Guo, *Macromolecules*, 2010, **43**, 7695–7704.
30 H. F. Lee, S. W. Kuo, C. F. Huang, J. S. Lu, S. C. Chan and F. C. Chang, *Macromolecules*, 2006, **39**, 5458–5465.
31 W. C. Chen, S. W. Kuo, U. S. Jeng and F. C. Chang, *Macromolecules*, 2008, **41**, 1401–1410.
32 W. C. Chen, S. W. Kuo, C. H. Lu, U. S. Jeng and F. C. Chang, *Macromolecules*, 2009, **42**, 3580–3590.
33 W. C. Chen, S. W. Kuo and F. C. Chang, *Polymer*, 2010, **51**, 4176–4184.
34 I. H. Lin, S. W. Kuo and F. C. Chang, *Polymer*, 2009, **50**, 5276–5287.
35 J. G. Li, Y. D. Lin and S. W. Kuo, *Macromolecules*, 2011, **44**, 9295–9309.
36 J. G. Li, C. Y. Chuang and S. W. Kuo, *J. Mater. Chem.*, 2012, **22**, 18583–18595.
37 J. G. Li, W. C. Chu, U. S. Jeng and S. W. Kuo, *Macromol. Chem. Phys.*, 2013, **214**, 2115–2123.
38 W. C. Chu, J. G. Li and S. W. Kuo, *RSC Adv.*, 2013, **3**, 6485–6498.
39 C. C. Liu, J. G. Li, W. C. Chu and S. W. Kuo, *Macromolecules*, 2014, **47**, 6389–6400.
40 C. W. Chiou, Y. C. Lin, L. Wang, T. Hayakawa and S. W. Kuo, *Macromolecules*, 2014, **47**, 8709–8721.
41 Y. C. Wu, B. P. Bastakoti, M. Pramanik, Y. Yamauchi and S. W. Kuo, *Polym. Chem.*, 2015, **6**, 5110–5124.
42 J. Kwak, S. H. Han, H. C. Moon, J. K. Kim, V. Pryamitsyn and V. Ganesan, *Macromolecules*, 2015, **48**, 6347–6352.
43 J. Kwak, S. H. Han, H. C. Moon, J. K. Kim, J. Koo, J. S. Lee, V. Pryamitsyn and V. Ganesan, *Macromolecules*, 2015, **48**, 1262–1266.
44 V. Pryamitsyn, S. H. Han, J. K. Kim and V. Ganesan, *Macromolecules*, 2012, **45**, 8729–8742.
45 S. H. Han, V. Pryamitsyn, D. Bae, J. Kwak, V. Ganesan and J. K. Kim, *ACS Nano*, 2012, **6**, 7966–7972.
46 S. H. Han, J. K. Kim, V. Pryamitsyn and V. Ganesan, *Macromolecules*, 2011, **44**, 4970–4976.
47 J. Zhou and A. C. Shi, *J. Chem. Phys.*, 2009, **130**, 234904.
48 L. Wang, J. Lin and X. Zhang, *Polymer*, 2013, **54**, 3427–3442.
49 C. Tang, S. M. Hur, B. C. Stahl, K. Sivanandan, M. Dimitriou, E. Pressly, G. H. Fredrickson, E. J. Kramer and C. J. Hawker, *Macromolecules*, 2010, **43**, 2880–2889.
50 Y. Zhuang, L. Wang and J. Lin, *J. Phys. Chem. B*, 2011, **115**, 7550–7560.
51 A. Noro, M. Hayashi and Y. Matsushita, *Soft Mater.*, 2012, **8**, 6416–6429.
52 M. M. Coleman, J. F. Graf and P. C. Painter, *Specific Interactions and the Miscibility of Polymer Blends*, Technomic Publishing, Lancaster, PA, 1991.
53 S. W. Kuo, C. L. Lin and F. C. Chang, *Polymer*, 2002, **43**, 3943–3949.
54 S. W. Kuo, C. H. Wu and F. C. Chang, *Macromolecules*, 2004, **37**, 192–200.
55 C. H. Lu, C. F. Huang, S. W. Kuo and F. C. Chang, *Macromolecules*, 2009, **42**, 1067–1078.
56 C. H. Lu, S. W. Kuo, W. T. Chang and F. C. Chang, *Macromol. Rapid Commun.*, 2009, **30**, 2121–2127.
57 Y. S. Lu and S. W. Kuo, *RSC Adv.*, 2014, **4**, 34849–34859.
58 J. J. Chiu, B. J. Kim, E. J. Kramer and D. J. Pine, *J. Am. Chem. Soc.*, 2005, **127**, 5036–5037.
59 B. J. Kim, J. Bang, C. J. Hawker and E. J. Kramer, *Macromolecules*, 2006, **39**, 4108–4114.
60 S. C. Park, B. J. Kim, C. J. Hawker, E. J. Kramer, J. Bang and J. S. Ha, *Macromolecules*, 2007, **40**, 8119–8124.
61 J. J. Chiu, B. J. Kim, G. R. Yi, J. Bang, E. J. Kramer and D. J. Pine, *Macromolecules*, 2007, **40**, 3361–3365.
62 B. J. Kim, G. H. Fredrickson and E. J. Kramer, *Macromolecules*, 2008, **41**, 436–447.
63 P. H. Tung, S. W. Kuo, K. U. Jeong, S. Z. D. Cheng, C. F. Huang and F. C. Chang, *Macromol. Rapid Commun.*, 2007, **28**, 271–275.
64 P. H. Tung, S. W. Kuo, S. C. Chen, C. L. Lin and F. C. Chang, *Polymer*, 2007, **48**, 3192–3200.
65 S. W. Kuo, P. H. Tung and F. C. Chang, *Macromolecules*, 2006, **39**, 9388–9395.
66 T. K. Kwei, *J. Polym. Sci., Polym. Lett. Ed.*, 1984, **22**, 307–313.
67 Y. S. Lu, C. Y. Yu, Y. C. Lin and S. W. Kuo, *Soft Mater.*, 2016, **12**, 2288–2300.
68 R. J. Roe, *Methods of X-ray and Neutron Scattering in Polymer Science*, Oxford University Press, New York, 2000.
69 K. R. Shull, *Macromolecules*, 1992, **25**, 2122–2133.
70 S. W. Kuo, *J. Polym. Res.*, 2008, **15**, 459–486.
71 S. W. Kuo and F. C. Chang, *Macromolecules*, 2001, **34**, 4089–4097.